

## GEOMETRIC NONLINEAR AEROELASTIC ANALYSIS OF HIGH ASPECT RATIO WINGS

Omar S.Habib<sup>1</sup>, Mohammad N.AbuelFoutouh<sup>2</sup>, Hani.M.Negm<sup>3</sup>

Cairo University  
Giza, Egypt

### ABSTRACT

This paper aims to study the geometric non-linear aeroelastic behavior of high aspect ratio wings (HARW) using finite element Euler-Bernoulli beam model. The proposed aeroelastic model utilizes the updated Lagrangian formulation for structure modeling, while the aerodynamics is modeled using two methods for steady analysis (Static); 1-Strip theory, and 2- Vortex Lattice method (VLM), and the Theodorsen's strip theory for the unsteady analysis (Flutter). A numerical example is given, and the unique phenomena associated with non-linear aeroelasticity of HARW are discussed, explained, and compared with another published work. The importance of this work comes from its interpretations to these phenomena.

### INTRODUCTION

Modern aircraft are characterized by their high flexibility, specially the unmanned air vehicles (UAVs) which are used for high-altitude long-endurance missions. These UAVs have high aspect ratio wings that may deform dramatically during nominal flight conditions. So linear aeroelastic analysis can't be adopted, and non-linear analysis is a must. The work of [Patil, M.J, Hodges, D.H, and Cesnik, C.E, 2001] can be considered as the first to address this problem. Their work is based on the mixed variational formulation derived by [Hodges, D.H, 1990] as the structural model, and the finite-state induced flow model derived by [Peters, D.A, and Jansons, M.J, 1995] as the aerodynamic model. Also several research papers have been published in recent years studying this problem like the work of [S, W. and Cesnik, C.E., 2010] that shows how high flexibility leads to a strong coupling between the rigid body degrees of freedom and the elastic degrees of freedom which will in turn affects the overall aeroelastic instability of the aircraft. The main difficulty that may face a researcher encountering this problem for the first time is the complexity of these models, therefore one of the objectives of this paper is to study and analyze the geometric nonlinear aeroelasticity of HARW using a more simple approach. The other objective is to provide some explanations for the unique phenomena associated with it, and hence help to understand its nature. So a non-linear aeroelastic model will be presented first, and then applied to a HARW. The results are compared to those of [Patil, M.J, Hodges, D.H, and Cesnik, C.E, 2001].

---

<sup>1</sup> Teaching Assistant in the Aerospace Engineering Department,Cario University Email: omarshukry@yahoo.com.

<sup>2</sup> Professor in the in the Aerospace Engineering Department,Cario University Email: naderabuelfoutouh@yahoo.com.

<sup>3</sup> Professor in the in the Aerospace Engineering Department,Cario University.

## AEROELASTIC MODELING

The geometric nonlinearity can be modeled using the updated Lagrangian formulation given by [Bathe, K.J, and Bolourchi, S., 1979]. The incremental time stepping technique is adopted by assuming that the structure's geometry and properties are known at time  $t$  and it is desired to solve the system at time  $t + \Delta t$ . So applying the principle of virtual work to the system at time  $t + \Delta t$ , the governing equation can be written as:

$$\int_{tV} {}^{t+\Delta t}S_{ij} \delta {}^{t+\Delta t}\epsilon_{ij} {}^t dV = {}^{t+\Delta t}\mathcal{F} \quad (1)$$

Where  $S_{ij}$  is the 2<sup>nd</sup> Piola-Kirchhoff stress, and  $\epsilon_{ij}$  is the Green-Lagrange strain which can be written in term of the displacement vector "u" as:

$${}^{t+\Delta t}\epsilon_{ij} = \frac{1}{2} ({}^{t+\Delta t}u_{i,j} + {}^{t+\Delta t}u_{j,i} + {}^{t+\Delta t}u_{k,i} {}^{t+\Delta t}u_{k,j}) \quad (2)$$

$\mathcal{F}$  is the external virtual work which can be written as:

$${}^{t+\Delta t}\mathcal{F} = \int_{{}^{t+\Delta t}S} {}^{t+\Delta t}\mathcal{f}_i^s \delta u_i^s {}^{t+\Delta t}dS + \int_{{}^{t+\Delta t}V} {}^{t+\Delta t}\mathcal{f}_i^b \delta u_i {}^{t+\Delta t}dV \quad (3)$$

Where  $\mathcal{f}^s$  is the surface traction vector,  $\mathcal{f}^b$  is the body force vector,  $S$  is the surface area, and  $V$  is the body volume. The left subscript indicates the reference configuration to which all variable are referred to, while the left superscript indicates the time at which a variable is measured. Applying linearization process, and then utilizing the finite element technique with the assumptions of the Euler-Bernoulli beam model as in [Bathe, K.J, and Bolourchi, S., 1979], the following system of equations is obtained:

$${}^{t+\Delta t}{}_t[K] {}^{t+\Delta t}\{\Delta q_s\} = {}^{t+\Delta t}\{F_s\}_{ext} - {}^t\{F_s\}_{int} \quad (4)$$

Where  ${}^{t+\Delta t}{}_t[K]$  is called the tangent stiffness matrix which consists of a linear part and a non-linear part as follows:

$${}^{t+\Delta t}{}_t[K] = ({}^{t+\Delta t}{}_t[K_L] + {}^{t+\Delta t}{}_t[K_{NL}]) \quad (5)$$

${}^{t+\Delta t}\{\Delta q_s\}$  is the incremental nodal displacement vector,  ${}^{t+\Delta t}\{F_s\}_{ext}$  is the external load vector at time  $t + \Delta t$ , and  ${}^t\{F_s\}_{int}$  is the internal force vector from the previous time step  $t$ . It is assumed that the structure will experience large deformation but small strain; which will lead to constant constitutive relations, which in turn, allows the length and the cross sectional area of each element to remain unchanged during the deformation.

Then the total displacement at any time can be obtained by adding the incremental displacement vectors up to that time as follows:

$${}^{t+\Delta t}\{q_s\} = {}^t\{q_s\} + {}^{t+\Delta t}\{\Delta q_s\} \quad (6)$$

The external load vector is evaluated from the applied aerodynamic load which has been estimated using two methods; Strip Theory (2D), and the Vortex lattice method (VLM) found in [Katz, J., and Plotkin, A., 2001]. Linear interpolation is used to couple the aerodynamic mesh and the structure mesh. Substituting in Eq.(3) the following static aeroelastic equilibrium equation is obtained:

$$\left({}^{t+\Delta t}{}^t[K] - {}^{t+\Delta t}q_\infty {}^{t+\Delta t}{}^t[A]\right){}^{t+\Delta t}\{\Delta q_s\} = {}^{t+\Delta t}q_\infty {}^{t+\Delta t}{}^t[A] {}^t\{q_s\} + {}^{t+\Delta t}\{f\} - {}^t\{F_s\}_{int} \quad (7)$$

Where  $q_\infty$  is the free stream dynamic pressure, and  $[A]$  is the aerodynamic stiffness matrix. The first term on the right-hand side is the aerodynamic load due to the displacement up to time  $t$ , while  $\{f\}$  represents the aerodynamic loads due to initial parameters such as the wing incidence, or other initial loads like the wing weight, which is very important when analyzing very flexible wings. The increment in loading is made by incrementing the free-stream Speed. This increment will be taken small, so it is not necessary to perform iteration to insure equilibrium at each loading step. Due to equilibrium, it can be noticed that the internal force vector equals the external load vector at the previous time step. So the static aeroelastic equilibrium equation can be written as:

$$\left({}^{t+\Delta t}{}^t[K] - {}^{t+\Delta t}q_\infty {}^{t+\Delta t}{}^t[A]\right){}^{t+\Delta t}\{\Delta q_s\} = ({}^{t+\Delta t}q_\infty - {}^tq_\infty){}^{t+\Delta t}{}^t[A] {}^t\{q_s\} + {}^{t+\Delta t}\{\Delta f\} \quad (8)$$

It should be noted that the components of the out-of-plane deformation (Twist Angles) in the deformation vector  ${}^{t+\Delta t}\{q_s\}$  calculated from Eqs.(6,8) are relative to the configuration at time  $t$ , so a transformation to the new configuration at time  $t + \Delta t$  is needed after each loading step. If small loading increments are used, then this transformation may be skipped without any significant effect on the results.

In order to address the flutter phenomenon, the standard U-g method as in [Bisplinghoff, R., Ashly, H., and Halfmann, R.L, 1955] is used to check the flutter speed after each loading step. If the estimated flutter speed equals the current free-stream speed then, it is the actual flutter speed. Using the U-g method will lead to the following Eigen- value problem:

$$\left({}^t[K]^{-1}({}^t[M] + {}^t[\mathcal{A}])\right)\{\Delta \bar{q}_s\} = \left(\frac{1 + ig}{\omega^2}\right)\{\Delta \bar{q}_s\} \quad (9)$$

Where  $[M]$  is the mass matrix,  $[\mathcal{A}]$  is the unsteady aerodynamic matrix (which contains stiffness, damping, and inertia components) which is computed using the Theodorsen's strip theory illustrated in [Bisplinghoff, R., Ashly, H., and Halfmann, R.L, 1955],  $g$  is an artificial damping factor, and  $\omega$  is the oscillation frequency. The shape functions used in the calculation of the stiffness matrix and the mass matrix to describe the displacement field were also used in the interpolation between the aerodynamic and the structure meshes.

## RESULTS AND DISCUSSION

The previous aeroelastic model has been applied to the HARW given in [Patil, M.J, Hodges, D.H, and Cesnik, C.E, 2001] using 32 beam elements and 1m/s increment in the free-stream velocity. The wing properties are given in Table (1).

Table 1: Properties of the High Aspect Ratio Wing.

Semi-Span(m)	16
Chord (m)	1
Sweep angle (deg)	0
Mass per unit length (Kg/m)	0.75
Mass Moment of inertia per unit length (at 50% of chord) (Kg.m)	0.1
Elastic axis position (%of chord)	50
Center of gravity position(%of chord)	50
Bending stiffness (N.m <sup>2</sup> )	2 (10) <sup>4</sup>
Torsion stiffness(N.m <sup>2</sup> )	1 (10) <sup>4</sup>
Air density (Kg/m <sup>3</sup> )	0.0889

The static analysis results are shown in Figures (1-4). Figures (1, 2) show the configurations of the wing half-span at different loading steps (Free-stream speeds) using 2D aerodynamics (Strip Theory) and the VLM respectively, for 4° initial angle of attack. It can be noticed that although the wing has a very high aspect ratio, the strip theory and the VLM can yield very different results. For example, at 25m/s free-stream speed, the strip theory yields nearly a 7m wing-tip displacement, while the VLM yields only 4.5 m wing-tip displacement, which means a 55% error.

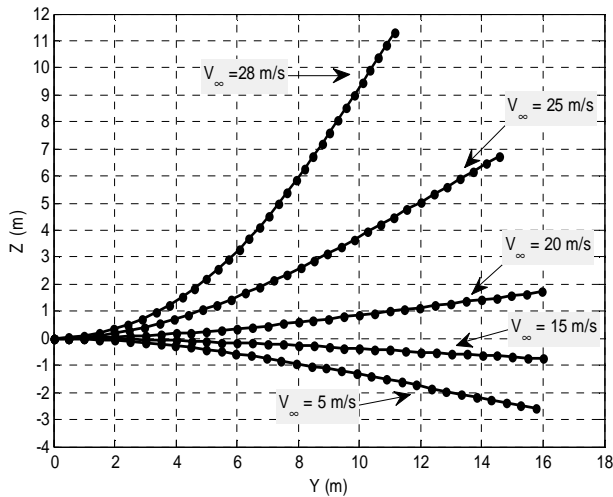


Figure 1: Configurations of the Wing Half-Span at Different Loading Steps Based on the Strip Theory.

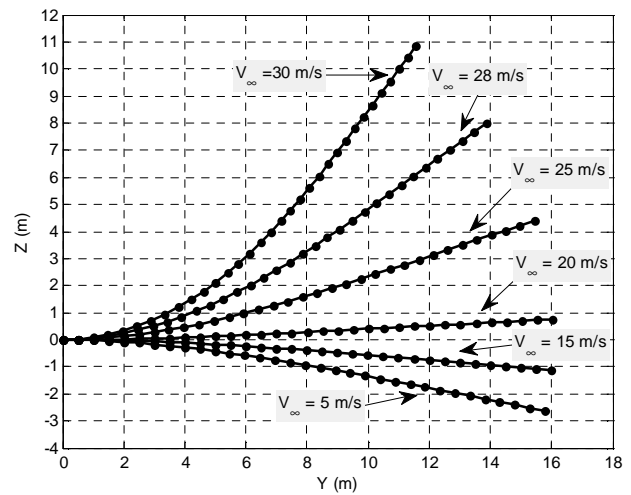


Figure 2: Configurations of the Wing Half-Span at Different Loading Steps Based on the VLM.

This difference in the results of the two aerodynamic methods can be justified by Figure (3) that shows the lift distribution over the wing half-span for the undeformed state estimated by the two methods. It can be noticed that the strip theory estimates larger loading near the wing tip where the effect of loading on the elastic deformation is highest. So the two aerodynamic methods may give close total aerodynamic lift values for the case of a rigid wing, but they will definitely give different aeroelastic results at the same free-stream speed. This difference depends on several factors like; the initial angle of attack, the free-stream dynamic pressure, and the flexibility of the wing itself.

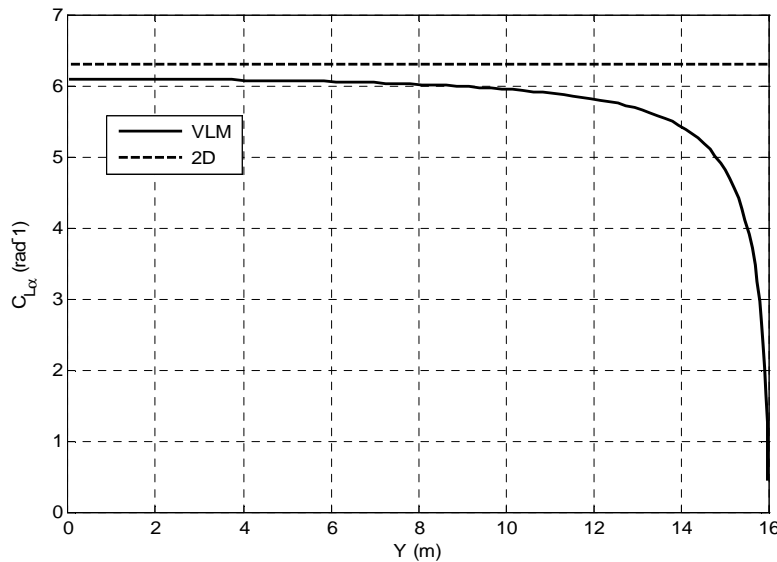


Figure 3: Lift Distribution Over the Wing Half-Span Estimated by the Strip Theory and the VLM.

Figure (4) shows the variation of the wing lift coefficient with the non-dimensional tip-displacement (displacement ratio) for 4° initial angle of attack. The figure shows that the maximum lift coefficient is reached at wing-tip displacement ratio around 0.3, but it should be noted that the maximum lift force is obtained at a higher value (around 0.5), since it depends also on the free-stream dynamic pressure. For the same tip-displacement, there is about 10% difference in the lift between the strip theory and the VLM.

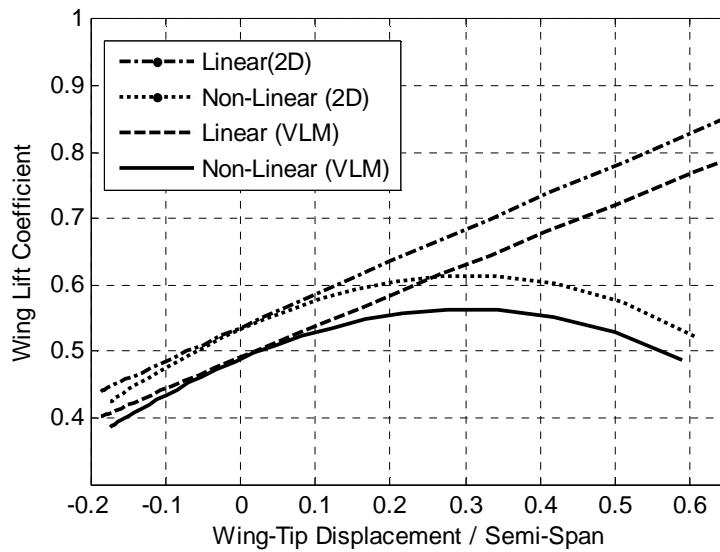


Figure (4): Variation of the Wing Lift Coefficient vs. the Non-Dimensional Tip Displacement.

The Flutter analysis results are shown in Figures (5-11). Figures (5, 6) show the variation of the estimated flutter speed and frequency vs. the free-stream speed for different initial angles of attack using 2D aerodynamics (similar curves can be obtained for the VLM case). The intersections between these curves and the free-stream speed line give the actual flutter speeds. The peaks in Figures (5, 6) represent the linear flutter speed and frequency

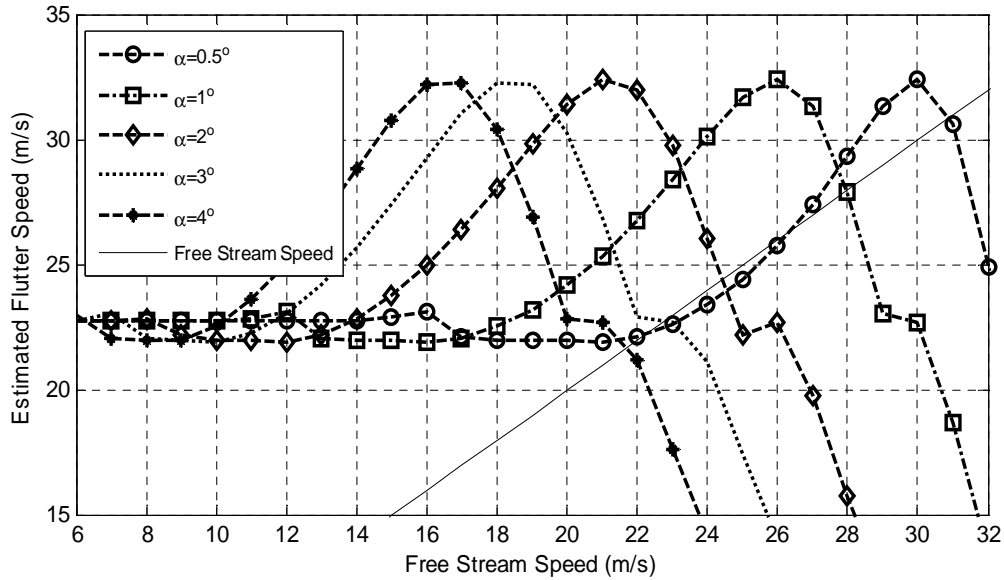
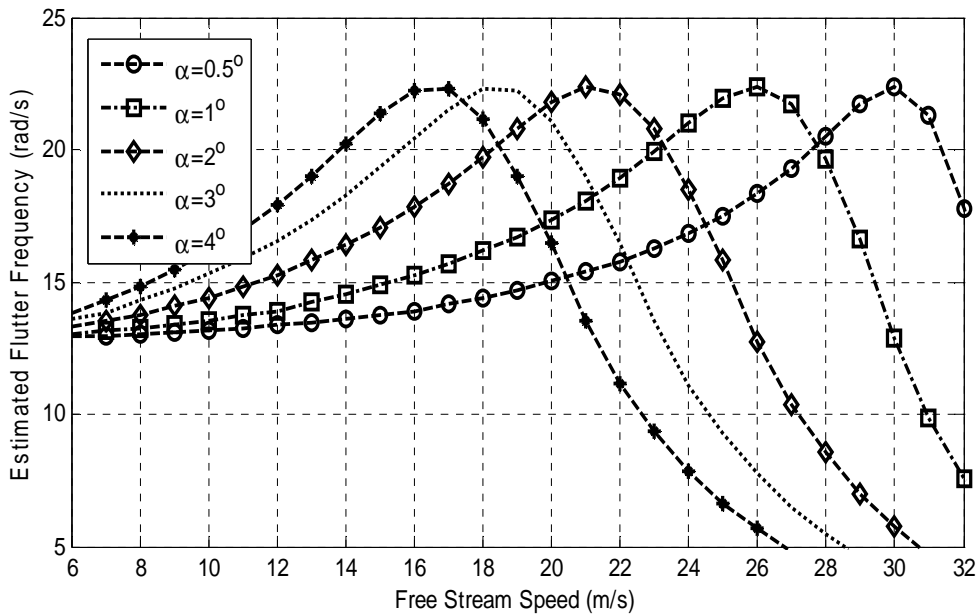


Figure (5): The Estimated Flutter Speed Vs. The Free-Stream Speed for Several Angles Of Attack (2D Aerodynamics).



Figure(6): The Estimated Flutter Frequency Vs. The Free-Stream Speed for Several Angles of attack (2D Aerodynamics).

Figures (7-8) show the variation of the flutter speed, flutter frequency, and the mean-tip displacement at flutter vs. the initial angle of attack. The results are compared to the results given in [Patil, M.J, Hodges, D.H, and Cesnik, C.E, 2001] .There are little differences between the two results in the range between (0°-3°) of initial angle of attack. [Patil, M.J, Hodges, D.H, and Cesnik, C.E, 2001] reported that the flutter speed and frequency will jump at an angle of attack around 4.5° to an off-scale value, while the analysis presented here shows a continuous decrease in the flutter speed and frequency.

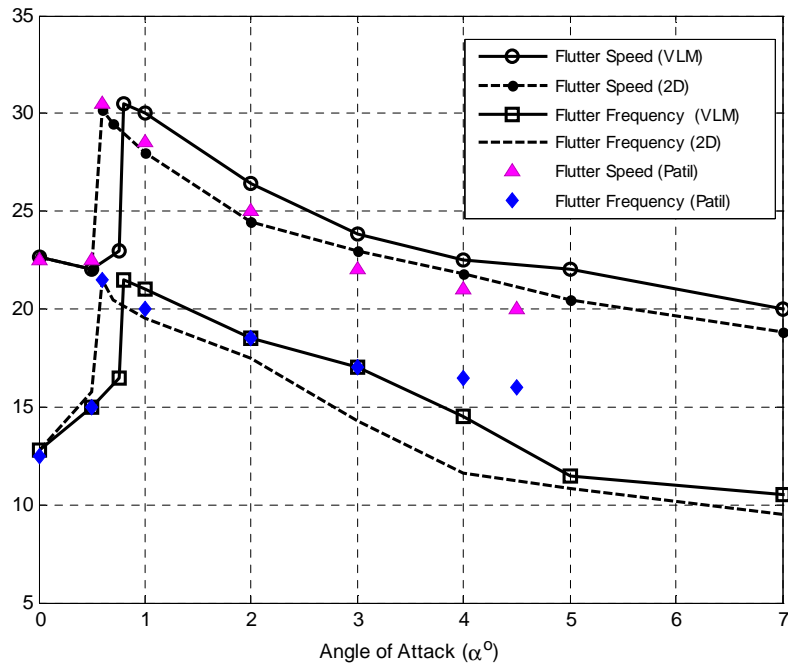


Figure (7): Variation of the Flutter Speed and Frequency vs. the Angle of Attack.

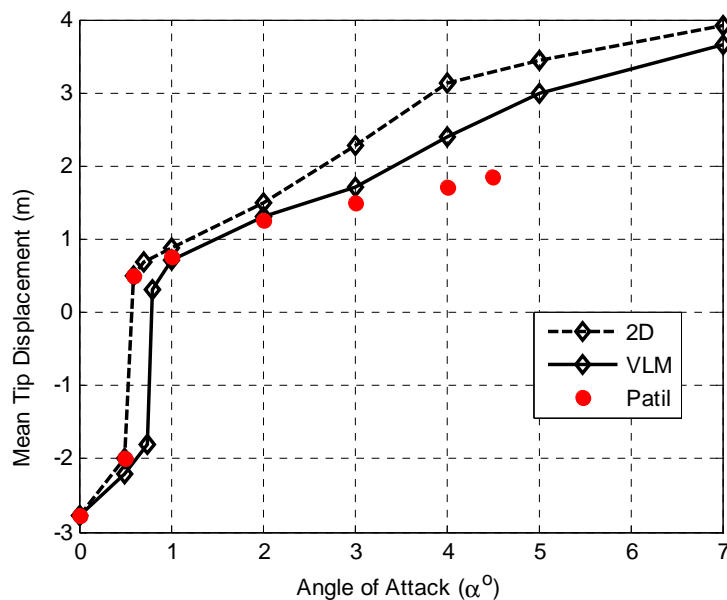


Figure (8) Variation of the Wing Mean Tip Displacement at Flutter vs. the Angle of Attack.

The jump in the flutter speed and frequency curves in Figure (7) at angle of attack  $0.6^\circ$  for the 2D aerodynamics case or at  $0.8^\circ$  for the VLM case can be justified as in [Patil, M.J, Hodges, D.H, and Cesnik, C.E, 2001] by Figure (9) that shows the flutter speed envelope of the wing vs. the wing-tip displacement (Bold line), and the variation of wing-tip displacement vs. the free-stream speed for  $0.6^\circ$  initial angle of attack (Dashed line). The two curves become tangent to each other at the first meeting point (Negative tip deflection) but do not intersect, but they intersect at the second meeting point (positive tip deflection). So for angles of attack lower than  $0.6^\circ$  the two curves will first intersect at a point with negative tip deflection, and for angles of attack higher than  $0.6^\circ$ , the two curves will intersect at a point with positive tip deflection.

The flutter envelope given in Figure (9) is wider than the one given in [Patil, M.J, Hodges, D.H, and Cesnik, C.E, 2001].

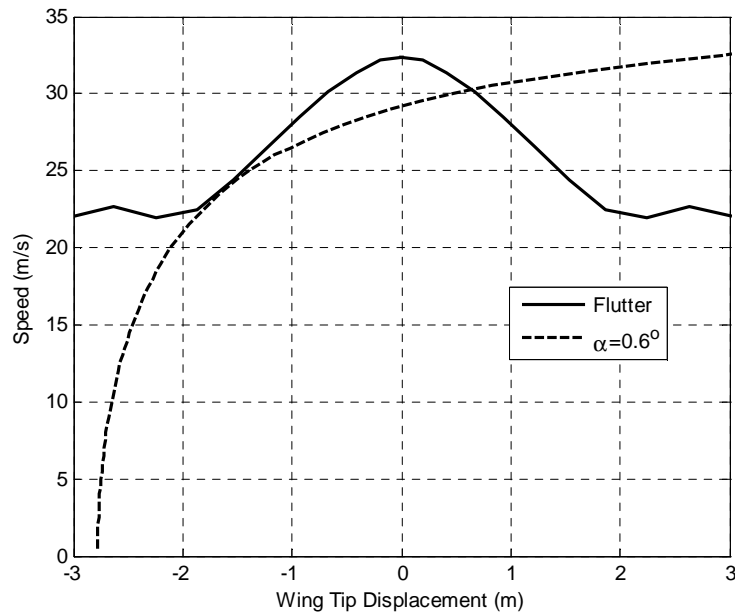


Figure (9): The Flutter Boundary Vs. The Wing Tip displacement (2DAerodynamics).

The reduction of the flutter speed and frequency as the wing deforms can be explained by Figure (10) that shows that the first torsion mode frequency decreases as the wing-tip displacement increases, while the first and second bending modes remain approximately constant. This decrease in the torsion frequency is due to the change of the torsion mode's nature. For the undeformed state the wing rotates about its elastic axis, but for the deformed state the wing rotates about the root section as shown in Figure (11). As the wing deforms, its center of mass is shifted upward causing its rotational inertia about the root to increase, causing a reduction in the torsion frequency. This explanation is different from the one given in [Patil, M.J, Hodges, D.H, and Cesnik, C.E, 2001] which states that the reduction of the torsion frequency is caused by a coupling between the torsion and the out-of-plane bending mode, which is thought to need reconsideration.

It can be noticed from Figure (10) that the first torsion mode intersects with the second bending mode at about 2.7 m wing-tip displacement causing a shift in the order of the natural modes. This shift may interpret the shifts seen in the estimated flutter curves in Figures (5, and 9) which all occur at 2.7m wing-tip displacement. Also [Patil, M.J, Hodges, D.H, and Cesnik, C.E, 2001] reported a faster decrease in the torsion frequency such that it intersects with the second bending mode frequency at around 2.1 m tip displacement.

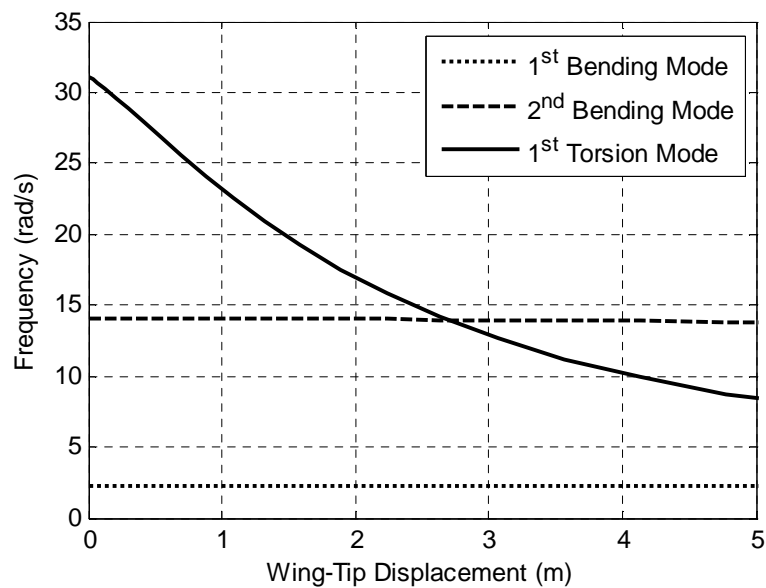


Figure (10): Variation of the Natural Frequencies vs. the Wing Tip Displacement.

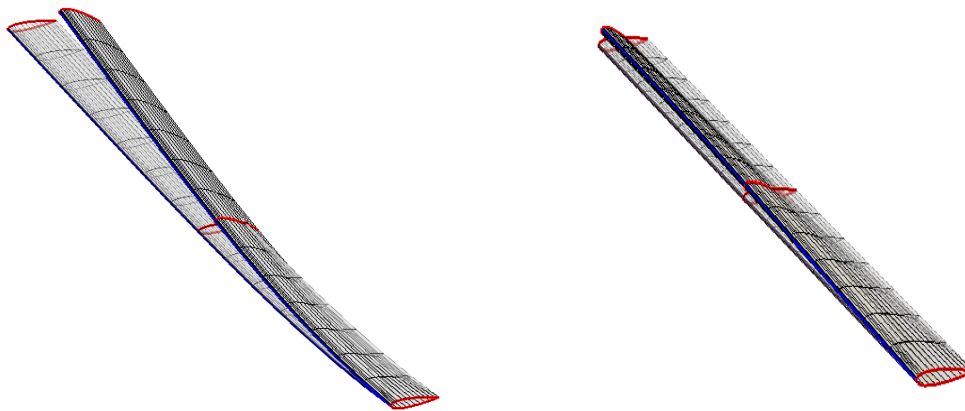


Figure (11): The First Torsion Mode Shape of the Undeformed Wing (right) and the Deformed Wing (left)

It can be noticed from Figure (11) that the torsion mode of the deformed wing contains an out-of-plane motion, and this motion increases as the wing deforms, which causes the drag force and the out-of-plane motion to have more effect on the aerodynamic loads and in turn the flutter results as the initial angle of attack increases. Since the Theodorsen's theory was used in this paper, then this effect wasn't taken into account.

## CONCLUSIONS

The aim of this paper was to study the geometric non-linear aeroelasticity of high aspect ratio wings. The finite element technique using an Euler-Bernoulli beam model was adopted. The updated Lagrangian formulation was used. Both the strip aerodynamic theory and the vortex lattice method were used for static analysis, while the Theodorsen's unsteady theory was used for the flutter analysis. The results showed that for static analysis 3D aerodynamic modeling is a must, even though the wing has a high aspect ratio. The geometric non-linearity can reduce the flutter speed and frequency dramatically. This reduction depends on the initial angle of attack of the wing. Also, this reduction results from the reduction of the wing's 1<sup>st</sup> torsion frequency as the wing deforms, while the bending frequencies remain approximately unchanged. The nature of the torsion mode of the deformed wing is different from that of the undeformed wing. For the undeformed wing the torsion mode is about the elastic axis, while for the deformed wing the torsion mode is about the root section. The effect of drag forces and the out-of-plane motion is thought to have a significant effect on flutter for high initial angle of attack, but this effect is not considered herein. Some interpretations presented here for the phenomena associated with the geometric non-linear aeroelasticity agree with the interpretations given in [Patil, M.J, Hodges, D.H, and Cesnik, C.E, 2001], but others don't. Besides some new aspects have been illustrated in the present work, which were not considered there. This work can be considered a first step towards understanding the geometric non-linear aeroelasticity of HARW without the need to use complex mathematical models.

## REFERENCES

- Bathe, K.J., and Bolourchi, S., (1979) "Large Displacement Analysis of Three- Dimensional Beam Structures", *International Journal for Numerical Methods in Engineering*, Vol.14, pp.961- 986,1979.
- Bisplinghoff, R., Ashly, H., and Halfmann, R.L., (1955) "Aeroelasticity", Dover Publications, 1955.
- Hodges, D.H., (1990) "A Mixed Variational Formulation based on Exact Intrinsic Equations for Dynamics of Moving Beams." *International Journal of Solids and Structures*, Vol.26 No.11, pp.1253-1273, 1990.
- Katz, J., and Plotkin, A., (2001) "Low-Speed Aerodynamics", 2<sup>nd</sup> edition, Cambridge University press, 2001.
- Patil, M.J., Hodges, D.H., and Cesnik, C.E.S., (2001) "Nonlinear Aeroelasticity and Flight Dynamics of High-Altitude Long Endurance Aircraft." *Journal of Aircraft*, Vol. 38, No.1, pp. 88-94, 2001.
- Peters, D. A. and Johnson, M. J., (1994) "Finite-State Air loads for Deformable Airfoils on Fixed and Rotating Wings," In *Symposium on Aeroelasticity and Fluid/Structure Interaction*, Proceedings of the Winter Annual Meeting. ASME, November, 1994.
- Su, W. and Cesnik, C.E, (2010), "Nonlinear Aeroelasticity of a Very Flexible Blended Wing-Body Aircraft." *Journal of Aircraft*, Vol.47, No.5 , pp.1539-1553, 2010.